Hindawi
Geofluids
Volume 2021, Article ID 9922653, 12 pages
https://doi.org/10.1155/2021/9922653

WILEY | Hindawi

Research Article

Analysis of Vertical Response of Drilled Pile at the Crest of Rock Slope Based on Shear Behavior

Chong Jiang, Ju Fang, and Bowen Sun

School of Resources and Safety Engineering, Central South University, Changsha, 410083 Hunan, China

Correspondence should be addressed to Chong Jiang; jiang4107@sohu.com

Received 31 March 2021; Accepted 8 May 2021; Published 26 May 2021

Academic Editor: Yu Wang

This paper proposed a method for analysis of a drilled pile under vertical load at the crest of rock slope. Based on wedge theory, a modified model of normal stiffness of socket wall affected by the slope is obtained. Analyze the shear behaviors of the pile-rock interface, an analytical solution of load transfer of pile at the crest of rock slope is obtained. To evaluate the accuracy of the new method, this method is compared with the results of finite difference analysis. Finally, the method is used to analyze the effect of slope, pile, and rock properties on the unit side resistance and axial force.

1. Introduction

Piles, which are widely used in offshore drillings, bridges, and other structures, are often embedded in rocks. Foundations constructed in level ground near continental, nearshore slopes, or man-made slope are inevitable in engineering practice. Because of slope, increase in settlement is observed [1, 2].

To analyze load transfer of pile under vertical loads, a series of method have been proposed. Laboratory test [3–7] could evaluate the vertical behaviors of pile; however, there are differences between small scale model pile test and engineering practice. Numerical method [1, 2, 8, 9] could simulate various engineering conditions, but parameters of sophisticated soil constitutive relations are hard to obtain. Theoretical method [10–23] could quickly obtain the relationship between load and settlement under various working conditions.

Jiang et al. [1, 2] used theoretical method to investigate the behaviors of rigid piles in sloping ground and obtained the effect of slope on the settlement. Jesmani et al. [24] investigated the effect of different types of clayey slopes on vertical bearing capacity based on finite element. All these methods applied to the soil slope; however, there are differences between soil and rock. For short pile in soil, structural loads are carried by base resistance, but for long pile embedded in rock, the bearing capacity almost depends on side resistance.

Johnston and Lam [25] analyzed pile-rock surface and proposed the theory of dilation energy. Based on the theory of dilation energy, many scholars [26–29] have studied the shear behavior of pile-rock interface. Zhao MH et al. [30], Xing HF et al. [31], and Zhao H [32] investigated the principal mechanisms of shear transfer between piles and rock, and the failure surfaces were assumed to line and slip-line field, respectively. All these methods obtained the effect of the concrete-rock surface on the behaviors. But for the pile at the crest of rock slope, because of slope, the normal stiffness of socket wall will decrease. To accurately evaluate the behaviors of pile at the crest of rock slope, the decrease of normal stiffness of socket wall is the key to the principal mechanisms of shear transfer between piles and rock.

To obtain the effect of slope on normal stiffness of socket wall, the wedge theory is used to illustrate it. An analytical solution of load transfer of pile at the crest of rock slope is obtained by analyzing the shear behaviors of the pile-rock interface. To evaluate the accuracy of the new method which is analysis of a drilled pile under vertical load at the crest of rock slope, this method is compared with the results of finite element analysis. Finally, the method is used to analyze the effect of slope, pile, and rock properties on the unit side resistance and axial force.

2. An Analytical Solution of Load Transfer of Pile at the Crest of Rock Slope considering the Shear Behaviors of the Pile-Rock Interface

2.1. Initial Normal Stiffness Equation Based on Wedge Theory. The basic assumptions of this paper are as follows: For the pile at the crest of rock slope, because of slope, the normal stiffness of socket wall will decrease. The schematic of the slope-pile model analyzed is illustrated in Figure 1. (x, z) is the Cartesian coordinate system, and the y direction is perpendicular to the x-z plane. The stress of the rock around the pile under the self-weight is ρg.

Based on the wedge stress theory, the three-direction stress relationship of rock under the self-weight at the crest of slope is:

$$\begin{cases} \sigma_z = \rho g z, \\ \sigma_x = \rho g z \dfrac{2 - 2\cos^2\gamma}{\cos^2\gamma}, \\ \sigma_y = \upsilon(\sigma_x + \sigma_z), \end{cases} \tag{1}$$

where σ_x, σ_y, and σ_z are the elastic stress solutions of the rock in the Cartesian coordinate system, υ is Poisson's ratio of rock, and γ is the complementary angle of α.

The initial tangent modulus equation of the pile at the crest of slope is:

$$E_0 = E_S(1 - \upsilon k_1 - \upsilon k_2), \tag{2}$$

where E_0 is the initial tangent modulus, E_S is the compression modulus, and k_1 and k_2 are the parameters defined as:

$$\sigma_x = k_1\sigma_z, \tag{3}$$

$$\sigma_y = k_2\sigma_z. \tag{4}$$

The initial tangent modulus equation of the pile in level ground is:

$$E_0{}' = \left(1 - \frac{2\upsilon^2}{1 - \upsilon}\right)E_s. \tag{5}$$

The normal restraint stiffness of the pile in level ground can be expressed as:

$$K' = \frac{E_0{}'}{(1 + \upsilon)r}, \tag{6}$$

where r is the radius of pile.

For the pile at the crest of rock slope, the normal stiffness of pile can be obtained by Eqs. (2)–(6):

$$K = R_{E_s}K', \tag{7}$$

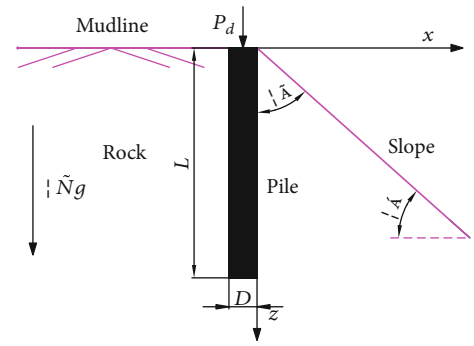

Figure 1: Schematic view of the slope-pile model.

where R_{E_s} is the ratio of the initial tangent modulus at the crest of slope to that in level ground; it can be expressed as:

$$R_{E_s} = \frac{(1 - \upsilon k_1 - \upsilon k_2)}{1 - (2\upsilon^2/(1 - \upsilon))}. \tag{8}$$

R_{E_s} is a function related to the Poisson's ratio υ, slope angle α, and embedded depth z. In order to obtain a more concise expression for $R_{E_s}(\alpha, \mathrm{z}, \upsilon)$, calculate the value of R_{E_s} in various situations.

Figure 2 shows the corresponding value of R_{E_s} when Poisson's ratio $\upsilon = 0.2, 0.25, 0.3, 0.35, 0.4$; slope angle $\alpha = 0, 2.5^\circ, 5^\circ, 7.5^\circ,...,30^\circ$; and embedded depths $z = 2\,\mathrm{m}, 4\,\mathrm{m}, 6\,\mathrm{m},...,20\,\mathrm{m}$. The distribution of R_{E_s} has a certain regularity, and it can obtained.

R_{E_s} is negatively correlated with the slope angle α and positively correlated with the Poisson's ratio of the rock. The equation for $R_{E_s}(\alpha, \mathrm{z}, \upsilon)$ was fitted by Matlab as:

$$R_{E_s}(\alpha, z, \upsilon) = \cos\left((1.654\upsilon + 0.129)\alpha\right). \tag{9}$$

For the pile at the crest of rock slope, the normal stiffness of pile can be obtained by Eqs. (7)–(9):

$$K = K' \cos\left((1.654\upsilon + 0.129)\alpha\right). \tag{10}$$

2.2. Shear Behavior of the Pile-Rock Interface

2.2.1. Assumption. Piles will be embedded in weathered rock of slopes, and its bearing capacity almost depends on side resistance. Relative slippage of concrete-rock interface occurs when the pile embedded in rocky slope is subjected to vertical load. Since the concrete-rock interface is rough, the slippage is often accompanied by radial expansion of the pile. The normal stress increases subsequently, and unit side resistance of pile is working. When pile embedded in slope is loaded, the sketch of relative shear motion of asperity is shown in Figure 3.

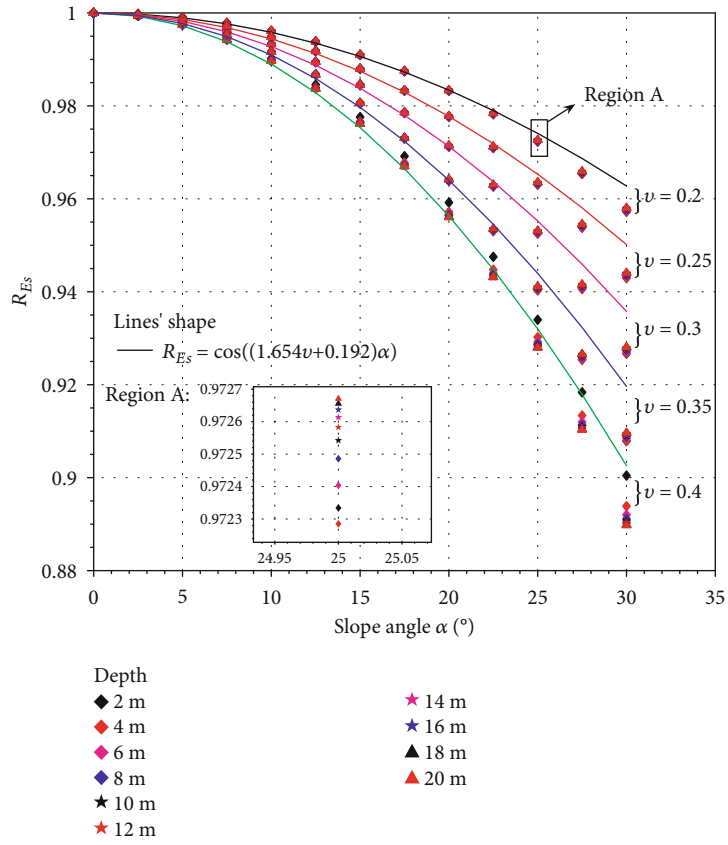

Figure 2: Fitting curve of R_{E_s}.

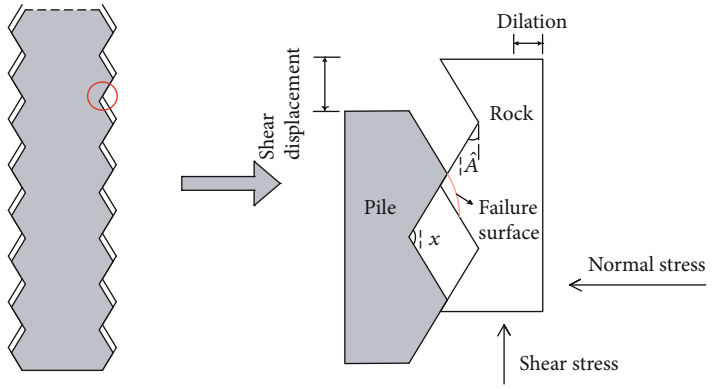

Figure 3: Shear motion of asperity.

To formulate shear behaviors of pile-rock interface and obtain solution of load transfer of pile at the crest of rock slope, assumptions of this paper are made in advance.

(1) The pile-rock interface with regular triangular asperity is consistent, and the inclination of asperity is β

(2) The cohesion of the pile-rock interface is small and cannot be accurately measured; the cohesion of the pile-rock interface is ignored. The initial normal stress could be ignored in the case of pile embedded in rocky slope because of a release of the initial geostatic stresses [33]

(3) The elastic modulus of the pile is greater than that of the rock; the surrounding rock is destroyed before the pile. The failure surface is curved, and the critical normal pressure of interface q_f can be expressed as

$$q_f = c \cot \varphi \left\{ \frac{1+\sin\varphi}{1-\sin\varphi} \exp\left[(2\psi-\pi)\tan\varphi\right] - 1 \right\}, \quad (11)$$

where c is the cohesion of rock, φ is the internal friction angle of rock, and ψ is vertex angle of regular triangle.

2.2.2. The Principal Mechanisms of Shear Transfer. The progress of shear behavior can be divided into dilation and residual periods. Dilation occurs when the shear displacement is small. With the development of the shear dilation, the pile-rock interface carries loads on the reach of critical stress, and the regular triangular asperity would be shorn off.

For the pile subjected to vertical load at the crest of rock slope, the slippage Δs is often accompanied with radial expansion of the pile Δr.

$$\Delta r = \Delta s \tan \beta, \tag{12}$$

where β is the dilation angle of rock.

And the normal stress will increase in the process of dilation; the incremental normal stress of pile-rock interface $\Delta\sigma_n$ can be expressed as:

$$\Delta\sigma_n = K' \cos\left((1.654\upsilon + 0.129)\alpha\right)\Delta r. \tag{13}$$

As mentioned in the previous assumption, the initial normal stress could be ignored. Therefore, stress acting normal to the direction along the pile σ_n can be expressed as:

$$\sigma_n = \Delta\sigma_n. \tag{14}$$

During progress of dilation, with the development of shear displacement, the normal stress increases continuously. Shear dilation for pile-rock interface is illustrated in Figure 4.

A classic theory for shear behavior is proposed, which was proposed by Patton et al. [34]. Shear stress for dilation can be expressed as:

$$\tau_d = \sigma_n \tan(\varphi_b + \beta), \tag{15}$$

where τ_d is the shear stress for dilation period and φ_b is the base friction angle of rock.

For the pile subjected to vertical load at the crest of rock slope, the unit side resistance for dilation can be obtained by Eqs. (12)–(15):

$$\tau_{(z)} = K' \cos\left((1.654\upsilon + 0.129)\alpha\right)s_{(z)} \tan\beta \tan(\varphi_b + \beta), \tag{16}$$

where $\tau_{(z)}$ is shear resistance for dilation at the depth z and $s_{(z)}$ is shear displacement at the depth z.

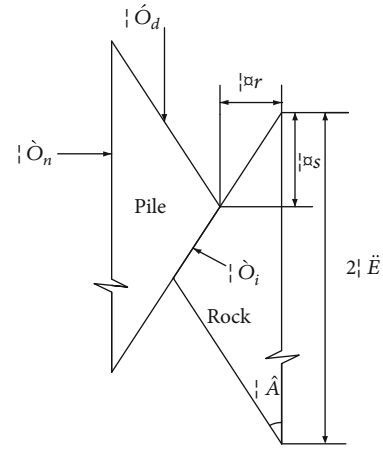

Figure 4: Schematic view of shear dilation for pile-rock interface.

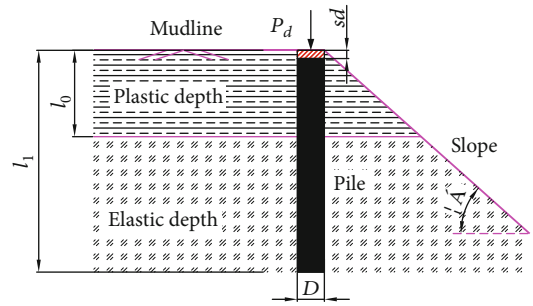

Figure 5: The sketch of plastic depth and elastic depth.

Table 1: The basic parameter values for verification.

Shaft diameter (D)	2.5 m
Shaft length (L)	32 m
Elastic modulus of pile (E_p)	30 GPa
Friction angle of interface (φ_b)	35°
Triangular half-chord length (λ)	3 mm
Cohesion of rock (c)	200 kPa
Internal friction angle of rock (φ)	25°
Elastic modulus of rock (E_r)	2.0 GPa
Poisson's ratio (υ)	0.25
Dilation angle of rock β	10°

With the development of the shear dilation, the pile-rock interface reaches the critical stress, and the regular triangular asperity would be shorn off. The condition of static equilibrium can be expressed as:

$$\frac{2\lambda(\sigma_n \cos\beta + \tau_d \sin\beta)}{(\lambda - \Delta s)} = \sigma_i, \tag{17}$$

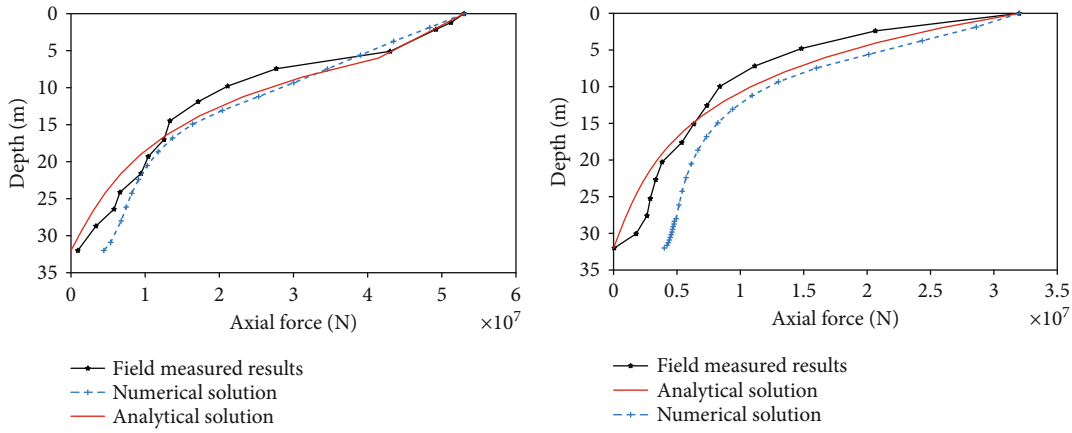

FIGURE 6: Verification in case of slope angle $\alpha = 0°$: (a) comparison in depth with 53 MN vertical load; (b) comparison in depth with 32 MN vertical load.

where λ is the triangular half-chord length, σ_i is the normal stress perpendicular to the pile-rock interface, and Δs is the slippage.

When the normal stress perpendicular to the pile-rock interface σ_i reaches the critical normal pressure of interface q_f, the condition of static equilibrium can be rewritten as:

$$\frac{2\lambda(\sigma_n \cos\beta + \tau_d \sin\beta)}{(\lambda - \Delta s_0)} = q_f, \tag{18}$$

where Δs_0 is the critical shear displacement.

As a result, the critical shear displacement Δs_0 can be obtained by Eqs. (12)–(15) and (18):

$$\Delta s_0 = \frac{\lambda q_f}{2\lambda K' \cos((1.654\upsilon + 0.129)\alpha) \tan\beta\{\cos\beta + [\tan(\varphi_b + \beta)\sin\beta]\} + q_f}. \tag{19}$$

The interface is plastic when the relative shear displacement $s_{(z)}$ is more than the critical shear displacement Δs_0. And the shear resistance for residual periods at the depth z would depend on residual parameters; the formulation of side resistance can be expressed as:

$$\tau_{(z)} = K' \cos((1.654\upsilon + 0.129)\alpha)\Delta s_0 \tan\beta \tan\varphi_r, \tag{20}$$

where φ_r is the residual friction angle of rock.

As a result, the equation of shear behavior for the pile subjected to vertical load at the crest of rock slope is generated as:

$$\tau_{(z)} = \begin{cases} K' \cos((1.654\upsilon + 0.129)\alpha) s_{(z)} \tan\beta \tan(\varphi_b + \beta) & \left(0 < s_{(z)} < \Delta s_0\right) \\ K' \cos((1.654\upsilon + 0.129)\alpha)\Delta s_0 \tan\beta \tan\varphi_r & \left(s_{(z)} > \Delta s_0\right) \end{cases}. \tag{21}$$

2.3. A Closed-Form Solution of Vertical Load Transfer of Pile at the Crest of Rock Slope

2.3.1. The Analytical Method of the Load Transfer. Generally speaking, the applied vertical load is supported by base resistance and side resistance. A number of related tests were conducted by scholars, and the experimental results illustrate that the bearing capacity almost depends on side resistance for long pile embedded in rock. For simplicity, the base resistance could be neglected in the case of pile embedded in rocky slope.

In this investigation, shear behavior can be distinguished into two periods. As illustrated by Eq. (21), the pile-rock interface would be behave plastic when the relative shear displacement $s_{(z)}$ is more than the critical shear displacement Δs_0. In contrast, the pile-rock interface would be in elastic.

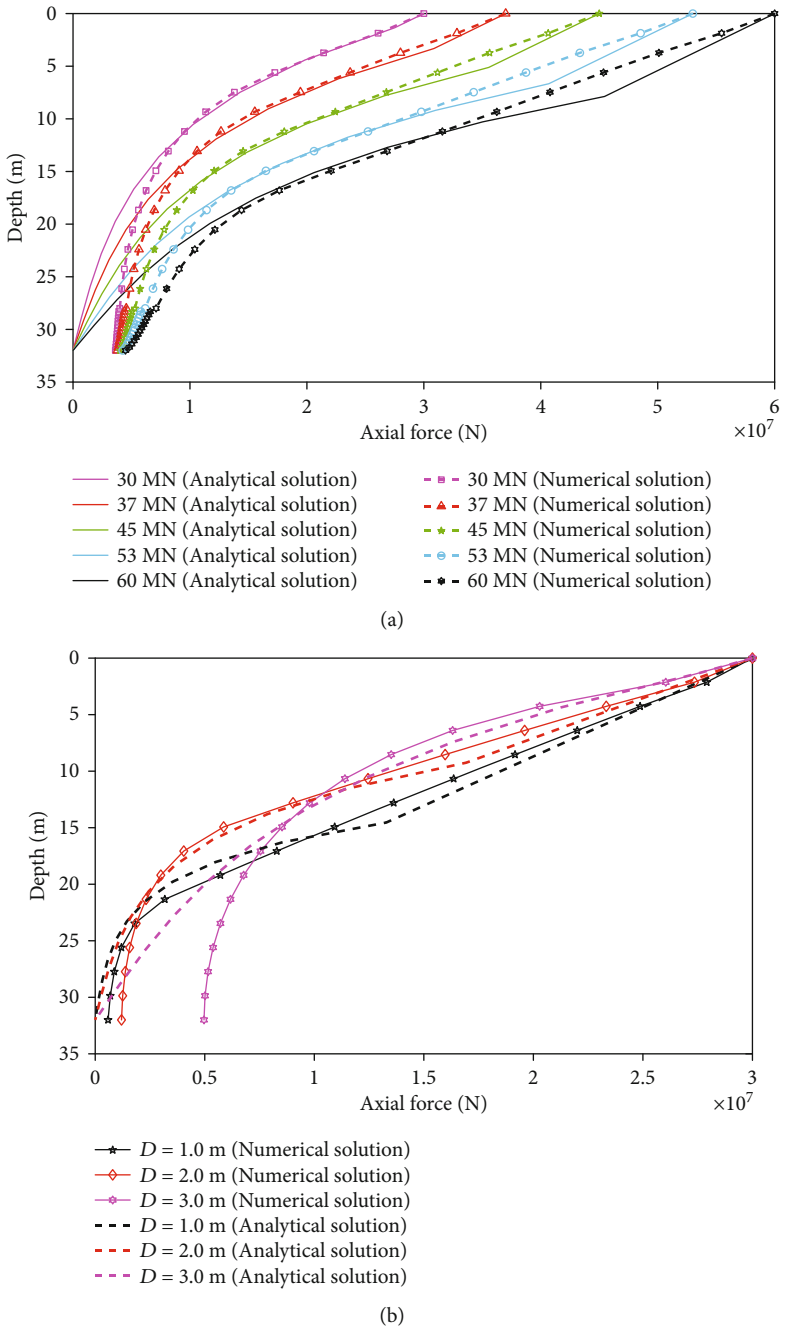

Figure 7: Verification in case of slope angle $\alpha = 30°$: (a) the axial force distributions with different vertical load; (b) the axial force distributions in different diameter of pile with 32 MN vertical load.

To depict the distribution of side resistance exactly, the analytical method of the load transfer has been used. It can combine the shear behavior of pile-rock interface with side resistance of pile, and the static equilibrium of unit pile under the vertical load can be expressed as:

$$\frac{d^2 s_{(z)}}{dz^2} = \frac{U}{E_p A_P} \tau_{(z)}, \tag{22}$$

where $s_{(z)}$ is the shear displacement at the depth z, U is the perimeter of pile, E_p is the elastic modulus of the pile, and A_P is the sectional area of the pile.

As illustrated in Figure 5, l_0 is the plastic depth, and l_1 is the elastic depth; s_d is settlement of pile top, and P_d is vertical load of pile top.

2.3.2. Solution of Plastic State. The pile-rock interface would be behave plastic when settlement of pile top s_d is more than

Table 2: The basic parameter values for parametric study.

Shaft diameter (D)	0.61 m
Shaft length (L)	6.1 m
Elastic modulus of pile (E_p)	27.6 GPa
Friction angle of interface (φ_b)	30°
Triangular half-chord length (λ)	8 mm
Cohesion of rock (c)	1.2 MPa
Internal friction angle of rock (φ)	24.8°
Elastic modulus of rock (E_r)	232 MPa
Poisson's ratio (υ)	0.3
Dilation angle of rock β	10°

the critical shear displacement Δs_0. The plastic solution for load transfer could be obtained by Eqs. (21) and (22):

$$\frac{d^2 s_{(z)}}{dz^2} = \frac{U}{E_p A_P} K' \cos\left((1.654\upsilon + 0.129)\alpha\right)\Delta s_0 \tan\beta \tan\varphi_r, \tag{23}$$

so, a general solution is expressed as:

$$s_{(z)} = \frac{UK' \cos\left((1.654\upsilon + 0.129)\alpha\right)\Delta s_0 \tan\beta \tan\varphi_r}{2E_p A_P} z^2 + c_1 z + c_2, \tag{24}$$

where c_1 and c_2 are constants.

The boundary conditions can be expressed as:

$$\begin{cases} s_{(z)}\Big|_{z=0} = s_d, \\ E_p A_p \dfrac{ds}{dz}\Big|_{z=0} = -P_d. \end{cases} \tag{25}$$

Substitution of Eq. (25) into Eq. (24) produces a solution:

$$\begin{cases} c_1 = \dfrac{-P_d}{E_p A_p}, \\ c_2 = s_d. \end{cases} \tag{26}$$

The plastic solution of vertical load in the case of pile embedded in rocky slope could be shown as:

$$s_{(z)} = \frac{UK' \cos\left((1.654\upsilon + 0.129)\alpha\right)\Delta s_0 \tan\beta \tan\varphi_r}{2E_p A_P} z^2 + \frac{-P_d}{E_p A_p} z + s_d, \tag{27}$$

$$\tau_{(z)} = K' \cos\left((1.654\upsilon + 0.129)\alpha\right)\Delta s_0 \tan\beta \tan\varphi_r, \tag{28}$$

$$P_{(z)} = P_d - UK' \cos\left((1.654\upsilon + 0.129)\alpha\right)\Delta s_0 \tan\beta \tan\varphi_r z. \tag{29}$$

The pile-rock interface is in conformity with continuity in displacements at the plastic depth l_0. It could be seen

$$s_{(l_0)} = \Delta s_0. \tag{30}$$

The plastic depth l_0 can be obtained by Eqs. (19), (27), and (30):

$$l_0 = \frac{\sqrt{{P_d}^2 + 2UK' \cos\left((1.654\upsilon + 0.129)\alpha\right)\Delta s_0 \tan\beta \tan\varphi_r E_p A_P (\Delta s_0 - s_d)} - P_d}{UK' \cos\left((1.654\upsilon + 0.129)\alpha\right)\Delta s_0 \tan\beta \tan\varphi_r}. \tag{31}$$

Substituting Eq. (31) into Eq. (29) produces

$$P_{(l_0)} = P_d - UK' \cos\left((1.654\upsilon + 0.129)\alpha\right)\Delta s_0 \tan\beta \tan\varphi_r l_0. \tag{32}$$

2.3.3. Solution of Elastic State. The pile-rock interface would be in elasticity below the plastic depth. As the previously analysis of shear behavior proposed, the solution of elastic state for load transfer could be obtained by Eqs. (21) and (22):

$$\frac{d^2 s_{(z)}}{dz^2} = \frac{UK' \cos\left((1.654\upsilon + 0.129)\alpha\right) \tan\beta \tan\left(\varphi_b + \beta\right)}{E_P A_P} s_{(z)}. \tag{33}$$

According to the statements introduced above, a general solution is expressed as:

$$s_{(z)} = c_3 e^{Rz} + c_4 e^{-Rz}, \tag{34}$$

where R, c_3, and c_4 are constant.

Substituting Eq. (34) into Eq. (33) produces

$$R = \sqrt{\frac{UK' \cos\left((1.654\upsilon + 0.129)\alpha\right) \tan\beta \tan\left(\varphi_b + \beta\right)}{E_P A_P}}. \tag{35}$$

The pile-rock interface is in conformity with continuity in axial force. And it can be expressed as:

$$\begin{cases} E_P A_P \dfrac{ds}{dz}\Big|_{z=l_0} = -P_{(l_0)}, \\ E_P A_P \dfrac{ds}{dz}\Big|_{z=l_1} = 0. \end{cases} \tag{36}$$

This leads to

$$s_{(z)} = \frac{P_d l_0 \cosh\left[R(l_1 - z)\right]}{RE_P A_P \sinh\left[R(l_1 - l_0)\right]}. \tag{37}$$

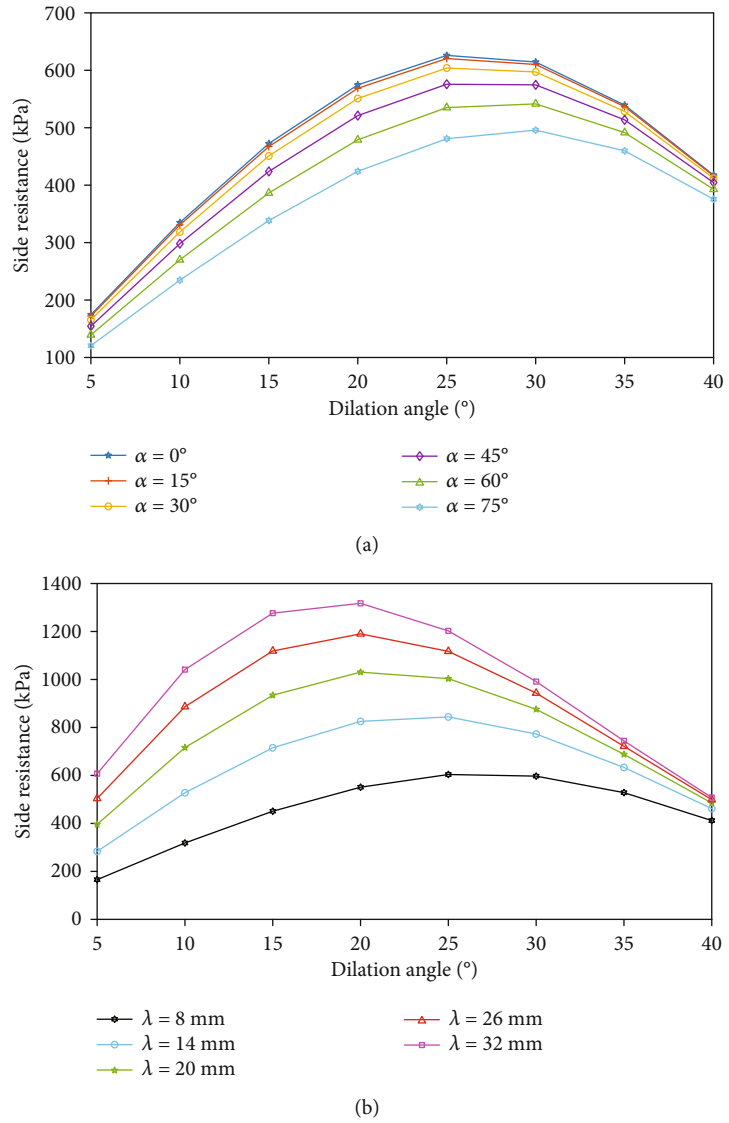

Figure 8: The influence of slope angle and interface roughness on residual unit side resistance: (a) the influence of slope angle; (b) the influence of the half-chord length.

The pile-rock interface is in conformity with continuity in displacements at the plastic depth l_0. It could be seen

$$\Delta s_0 = \frac{P_d l_0 \cosh\left[R(l_1 - l_0)\right]}{RE_P A_P \sinh\left[R(l_1 - l_0)\right]}. \tag{38}$$

The elastic depth l_1 can be expressed as

$$l_1 = R^{-1} \operatorname{arcoth}\left[\frac{RE_P A_P \Delta s_0}{P_{(l_0)}}\right] + l_0. \tag{39}$$

The elastic solution of vertical load in the case of pile embedded in rocky slope could be shown as:

$$\begin{aligned} \tau_{(z)} &= \frac{RP_{(l_0)} \cosh\left[R(l_1 - z)\right]}{U \sinh\left[R(l_1 - l_0)\right]}, \\ P_{(Z)} &= \frac{P_{(l_0)} \sinh\left[R(l_1 - z)\right]}{\sinh\left[R(l_1 - l_0)\right]}. \end{aligned} \tag{40}$$

3. Verification and Discussion

The mechanism of vertical load transfer is nonlinear and sophisticated for the pile at the crest of rock slope. It is difficult to study the progress of load transfer by conducting relative tests. To evaluate the accuracy of the new method, this method should be compared with the results of finite element analysis. The model of pile-slope is established with FLAC^{3D}. A pile embedded in the level ground for situ test was reported by Dong P et al. [35]. The basic parameter values of pile and slope for verification are showed in Table 1.

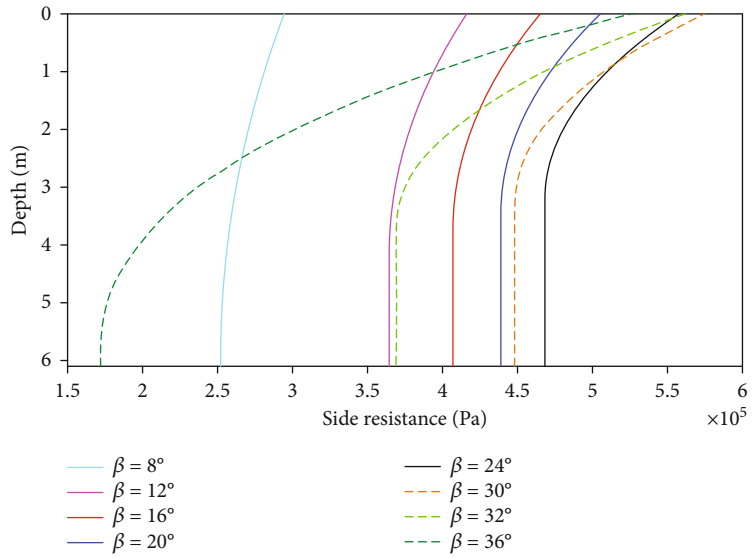

Figure 9: The influence of dilation angle on dilation unit side resistance.

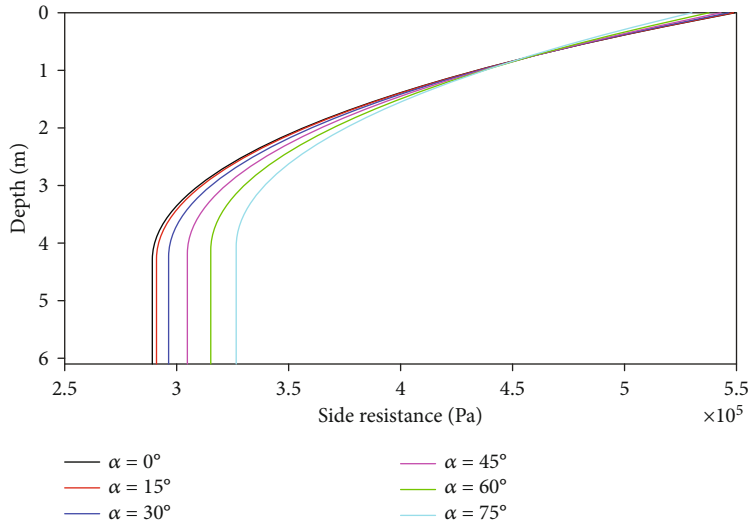

Figure 10: The influence of slope angle on dilation unit side resistance.

The reliability of the numerical simulation results should be demonstrated first. In case of slope angle $\alpha = 0^{\circ}$, the comparison of the results of numerical analysis, field measured results, and predict solution is shown in Figures 6 and 7.

Figure 6(a) illustrates the finite element results and the measured results of axial force distributions in depth with 53 MN vertical load. It is obvious that the regular triangular asperity has been shorn off, and part of the pile-rock interface has been in plasticity with 53 MN vertical load. The field measured result of the plastic depth l_0 is 5 m. By resolving the above equation, the plastic depth l_0 is 5.6 m, which matches closely with the field measured results. The numerical results of axial force distributions match more closely with the field measured results in the upper part of the pile. Figure 6(b) shows that the numerical results and the measured results of axial force distributions in depth with 32 MN vertical load. The numerical results of axial force distributions match closely with the field measured results. Since the base resistance has been neglected in analytical solution for simplicity, the base axial force of numerical results is larger than analytical results. Numerical simulation is more suitable to the actual working conditions, and the base resistance exists.

For the pile subjected to vertical load at the crest of rock slope, there are few relevant tests. Thus, the numerical method would be used to verify the accuracy of the theory.

In case of slope angle $\alpha = 30^{\circ}$, the comparison of the results of finite element analysis and predict solution is shown in Figure 7. As illustrated in Figure 7(a), the analytical results of axial force distributions match closely with the

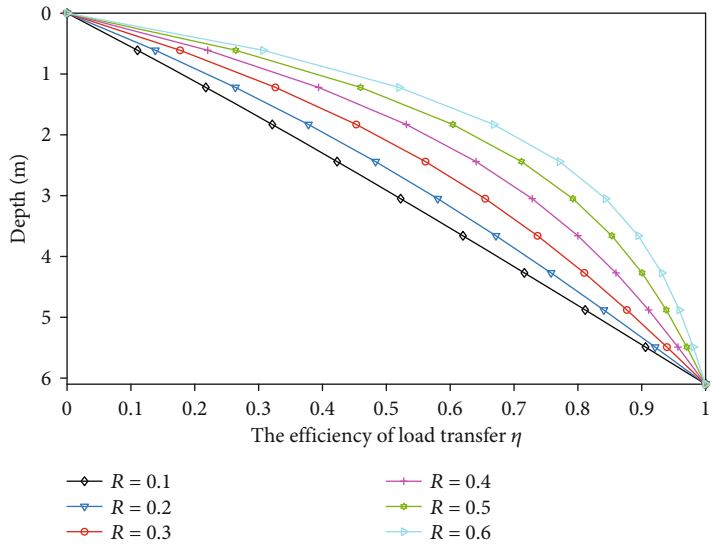

Figure 11: The influence of comprehensive parameters of slope-pile R on the efficiency of load transfer η.

numerical results in depth with any load. It is similar to the case of $\alpha = 0^\circ$ that the base axial force of numerical results is larger than analytical results. As explained in the previous section, the base axial force is 0 in analytical results while the base axial force exists in the actual engineering. The pile-rock interface would be in elastic when the vertical load is minimal. It would behave plastic when the vertical load is large enough, and the plastic depth l_0 would be larger with the increase of vertical load.

The highest axial force occurs in the upper part of the pile, which means the highest load transfer in the upper part of the pile correlates with highest values of shear displacements. The reduction of axial force is related to the shear displacement on the pile-rock interface. Figure 7(b) shows that the comparison of the results of finite element analysis and predict solution with different diameter of pile in case of $\alpha = 30^\circ$. It is obvious that the plastic depth l_0 has been larger with the reduction of diameter. And it seems that the higher load transfer in the upper part of the pile is associated with the smaller diameter. In other words, larger diameter piles have higher load carrying capacity.

In summary, the rationality of presented method has been explained by a series of numerical study for load transfer. And the analytical results of axial force distributions have a good match with the numerical results within the reasonable error range.

4. Parametric Study

There are many related parameters that affect the distribution of side resistance and axial force, especially for the vertical loaded pile at the crest of rock slope. Many scholars have focused on the issue of load transfer for pile at the level ground, and some conclusions are drawn. The effect of slope on the distribution of side resistance is an emphasis in this study. Therefore, a series of parametric analysis were conducted to further descript the presented method. The parametric study is investigated with the different parameters reported by O'Neill, as shown in Table 2.

4.1. Residual Period. The side resistance in plastic depth is constant, and it depends on the residual parameters and interface roughness. Figure 8 shows the effect of slope angle and roughness parameters on side resistance of residual periods in condition with 1296 kN vertical load. The values of half-chord length, dilation angle, and slope angle are varied from 8 mm to 32 mm, 5° to 40°, and 0° to 75°.

Figure 8(a) shows a tendency that the side resistance of residual periods decreases with the raised slope angle. At the same time, the higher slope angle, the greater reduction of the side resistance. This is because the larger slope angle, the smaller the normal constraint of pile. Figure 8(b) illustrates that the side resistance of residual periods increases and then decreases with the increase of dilation angle. It means that the simple increase of the dilation angle cannot enhance the side resistance; this may be caused by the quicker reduction of the contact area with the higher dilation angle. And it is obvious that the half-chord length is positively correlated with the side resistance.

4.2. Dilation Period. The value of side resistance in elastic depth is mobile on the method proposed previously, and the elastic depth is not immobile under different working conditions. As to the vertically loaded pile in dilation period, it is more difficult to descript the distribution of side resistance.

Figure 9 shows the effect of dilation angle on side resistance of dilation periods in condition of 4000 kN vertical load and 0.8 m diameter of pile. With the increase of dilation angle, the side resistance of dilation period increases initially and then decreases. This is similar to the behavior of residual period. As indicated previously, the smaller the dilation angle, the more uniform the distribution of side resistance. The values of dilation angle are varied from 8° to 36°.

Figure 10 illustrates the effect of slope angle on side resistance of dilation periods The values of slope angle are varied from 0° to 75°. The smaller the slope angle, the more concentrated the distribution of pile lateral friction at the top of the pile, the greater the decreasing rate of the side resistance, and the deeper the plastic depth. This may be caused by the normal constraint of pile is small when the slope angle is large. As a result, the slope angle would give engineers a guidance to optimize designs.

To further study the load transfer, the term of "efficiency of load transfer η" is referred in this paper. It can be expressed as $\eta = 1 - P_{(z)}/P_d$. According to the previous analysis of load transfer, R is a comprehensive parameter of slope pile. And it is a macroscopic composite index reflecting the bearing performance of pile embedded in the crest of the slope. Figure 11 illustrates the effect of comprehensive parameters of slope-pile R on the efficiency of load transfer η, and the values of R are varied from 0.1 to 0.6. The greater the R value, the greater the η value, and the upper pile bears more load. Therefore, the smaller the load ultimately transferred to the pile tip, the weaker the bearing capacity of the slope pile. As a result, the smaller R is beneficial to enhance the bearing capacity of piles.

5. Conclusion

In order to obtain the response of drilled pile under vertical load at the crest of rock slope. Efforts have been made in this paper to analysis the effect of slope on the normal stiffness of socket wall. The following conclusions can be drawn:

(a) A modified model of normal stiffness of socket wall affected by the slope is obtained; the effect of slope angle and Poisson's ratio on the reduce factor of normal stiffness of pile was proposed

(b) Analyze the shear behaviors of the pile-rock interface, an analytical solution of load transfer of pile at the crest of rock slope is obtained. The response of the drilled pile at the crest of rock slope was obtained from the closed-form solution

(c) The results of the new method were compared with the results of Flac^{3D}, which shows remarkable agreement

(d) The simple increase of the dilation angle cannot enhance the side resistance, and the half-chord length is positively correlated with the side resistance

(e) The side resistance of residual periods decreases with the raised slope angle, and the slope is a disadvantage for engineering. And the smaller comprehensive parameter of slope pile is beneficial to enhance the bearing capacity of piles

Data Availability

The data used to support the findings of this study are available from the corresponding author upon request.

Conflicts of Interest

The authors declare that there are no conflicts of interest regarding the publication of this paper.

Acknowledgments

This work is supported by the National Natural Science Foundation of China (Grant Nos. 51978665 and 51678570) and the Focus on research and development plan of Hunan province (No. 2015SK2053).

References

[1] C. Jiang, W. Y. Wu, J. L. He, and L. J. Chen, "Computation method for the settlement of a vertically loaded pile in sloping ground," *Advances in Civil Engineering*, vol. 2020, 10 pages, 2020.

[2] C. Jiang, Z. Zhang, and J. L. He, "Nonlinear analysis of combined loaded rigid piles in cohesionless soil slope," *Computers and Geotechnics*, vol. 117, p. 103225, 2020.

[3] M. W. O'Neill, K. M. Hassan, and F. C. Townsend, "Load transfer for drilled shafts in intermediate geomaterials," *FHWA-RD-95-172, Federal Highway Administration*, 1996McLean, VA, 1996.

[4] M. Sahara, N. Akino, and K. Tominaga, "Experimental results and elasto-plastic analysis of the vertical behavior of a single model pile," *Journal of Asian Architecture and Building Engineering*, vol. 1, no. 1, pp. 65–73, 2002.

[5] J. H. Chung, J. Ko, H. Klammler, M. C. McVay, and P. Lai, "A numerical and experimental study of bearing stiffness of drilled shafts socketed in heterogeneous rock," *Computers and Structures*, vol. 90-91, pp. 145–152, 2012.

[6] Y. Wang, Y. F. Yi, C. H. Li, and J. Q. Han, "Anisotropic fracture and energy characteristics of a Tibet marble exposed to multi-level constant-amplitude (MLCA) cyclic loads: a lab-scale testing," *Engineering Fracture Mechanics*, vol. 244, p. 107550, 2021.

[7] Z. Y. Song, Y. Wang, H. Konietzky, and X. Cai, "Mechanical behavior of marble exposed to freeze-thaw-fatigue loading," *International Journal of Rock Mechanics and Mining Sciences*, vol. 138, article 104648, 2021.

[8] R. Oliver, "Numerical study of the bearing behavior of piled rafts," *International Journal of Geomechanics*, vol. 4, no. 2, pp. 59–68, 2004.

[9] R. C. Liu, B. S. Xu, B. Li, and Y. J. Jiang, "3-D numerical study of mechanical behaviors of pile-anchor system," *Applied Mechanics and Materials*, vol. 580-583, pp. 238–242, 2014.

[10] H. B. Seed and L. C. Reese, "The action of soft clay along friction piles," *Transactions of the American Society of Civil Engineers*, vol. 122, no. 1, pp. 731–754, 1957.

[11] E. D'Appolonia and J. P. Romualdi, "Load transfer in end-bearing steel H-piles," *Journal of the Soil Mechanics and Foundations Division*, vol. 89, no. 2, pp. 1–25, 1963.

[12] H. M. Coyle and L. C. Reese, "Load transfer for axially loaded piles in clay," *Journal of the Soil Mechanics and Foundations Division*, vol. 92, no. 2, pp. 1–26, 1966.

[13] J. P. Carter and F. H. Kulhawy, "Analysis and design of drilled shaft foundations socketed into rock," EPRI EL-5918, Ithaca, New York, 1988.

[14] R. Radhakrishnan and C. F. Leung, "Load transfer behavior of rock-socketed piles," *Journal of Geotechnical Engineering*, vol. 115, no. 6, pp. 755–768, 1989.

[15] K. M. Hassan and M. W. O'Neill, "Side load-transfer mechanisms in drilled shafts in soft argillaceous rock," *Journal of Geotechnical Engineering*, vol. 123, no. 2, pp. 145–152, 1997.

[16] L. Zhang and H. H. Einstein, "End bearing capacity of drilled shafts in rock," *Journal of Geotechnical and Geoenvironmental Engineering*, vol. 124, no. 7, pp. 574–584, 1998.

[17] P. J. N. Pells, "State of practice for the design of socketed piles in rock," in *Proceedings of the Eighth Australia New Zealand conference on geomechanics. Australian Geomechanics Society*, pp. 307–327, Barton, ACT, 1999.

[18] C. Zhan and J. Yin, "Field static load tests on drilled shaft founded on or socketed into rock," *Canadian Geotechnical Journal*, vol. 37, no. 6, pp. 1283–1294, 2000.

[19] C. W. W. Ng, T. L. Y. Yau, J. H. M. Li, and W. H. Tang, "Side resistance of large diameter bored piles socketed into decomposed rocks," *Journal of Geotechnical and Geoenvironmental Engineering*, vol. 127, no. 8, pp. 642–657, 2001.

[20] K. Georgiadis, M. Georgiadis, and C. Anagnostopoulos, "Lateral bearing capacity of rigid piles near clay slopes," *Soils and Foundations*, vol. 53, no. 1, pp. 144–154, 2013.

[21] Q. Q. Zhang, R. F. Feng, Y. L. Yu, S. W. Liu, and J. G. Qian, "Simplified approach for prediction of nonlinear response of bored pile embedded in sand," *Soils and Foundations*, vol. 59, no. 5, pp. 1562–1578, 2019.

[22] B. Ma, Z. Hu, Z. Li et al., "A three-section-settlement calculation method for composite foundation reinforced by geogrid-encased stone columns," *Advances in Civil Engineering*, vol. 2021, 10 pages, 2021.

[23] B. Ma, Z. Li, K. Cai et al., "An improved nonlinear settlement calculation method for soft clay considering structural characteristics," *Geofluids*, vol. 2021, 7 pages, 2021.

[24] M. Jesmani, A. Kasrania, and M. Kamalzare, "Finite element modelling of undrained vertical bearing capacity of piles adjacent to different types of clayey slopes," *International Journal of Geotechnical Engineering*, vol. 12, no. 2, pp. 147–154, 2018.

[25] I. W. Johnston and T. S. K. Lam, "Shear behavior of regular triangular concrete/rock joints-analysis," *Journal of Geotechnical and Geoenvironmental Engineering*, vol. 115, no. 5, pp. 711–727, 1989.

[26] J. P. Seidel and C. M. Haberfield, "Towards an understanding of joint roughness," *Rock Mechanics and Rock Engineering*, vol. 28, no. 2, pp. 69–92, 1995.

[27] X. F. Gu, *Shear Behaviour of Sandstone-Concrete Joints and Pile Shafts in Sandstone, [Ph.D. thesis]*, Department of Civil Engineering, Monash University Australia, 2001.

[28] L. David Suits, T. C. Sheahan, J. P. Seidel, and C. M. Haberfield, "Laboratory testing of concrete-rock joints in constant normal stiffness direct shear," *Geotechnical Testing Journal*, vol. 25, no. 4, article 10416, 2002.

[29] B. M. Basha and G. L. S. Babu, "Seismic rotational displacements of gravity walls by pseudodynamic method with curved rupture surface," *International Journal of Geotechnical Engineering*, vol. 10, no. 3, pp. 93–105, 2010.

[30] M. H. Zhao, Y. Lei, and X. M. Liu, "Analysis of load transfer of rock-socketed piles based on characteristics of pile-rock structural plane," *Chinese Journal of Rock Mechanics and Engineering*, vol. 28, no. 1, pp. 103–110, 2009, [in Chinese].

[31] H. F. Xing, M. H. Meng, and W. Y. He, "Analysis of the distribution of side friction resistance of rock-socketed piles based on the mechanical characteristics of structural surfaces," *Chinese Journal of Geotechnical Engineering*, vol. 12, pp. 2220–2227, 2012.

[32] H. Zhao, Y. Xiao, M. Zhao, and P. Yin, "On behavior of load transfer for drilled shafts embedded in weak rocks," *Computers and Geotechnics*, vol. 85, pp. 177–185, 2017.

[33] S. Y. Liu, J. Peng, and W. Jie, "Load transfer behavior of large diameter cast-in-place pile embedded in soft rock," *Chinese Journal of Geotechnica1 Engineering*, vol. 20, no. 4, pp. 58–61, 1998, [in Chinese].

[34] F. D. Patton, "Multiple modes of shear failure in rock," in *Proceeding of the 1st Congress of International Society of Rock Mechanics*, Lisbon, Portugal, 1966.

[35] P. Dong, "Bearing behavior of large- diameter rock- socket piles," *Chinese Journal of Rock Mechanics and Engineering*, vol. 22, no. 12, pp. 2099–2103, 2003, [in Chinese].